NATIONAL TRANSPORTATION SAFETY BOARD

Office of Research and Engineering
Materials Laboratory Division
Washington, D.C. 20594

October 4, 2002

MATERIALS LABORATORY FACTUAL REPORT Report No. 02-078

A. ACCIDENT

Place	: Belle Harbor, New York
Date	: November 12, 2001
Vehicle	: Airbus A300-600, N14053
NTSB No.	: DCA02MA001
Investigator	: Brian Murphy, AS-40

B. COMPONENTS EXAMINED

Vertical stabilizer and rudder.

C. ACCIDENT SUMMARY

On November 12, 2001, at approximately 0917 EST, American Airlines flight 587, an Airbus A-300-600, N14053, crashed into a neighborhood in Belle Harbor, New York, several minutes after taking off from Kennedy International Airport. The airplane was on a scheduled flight to Santo Domingo, Dominican Republic. All 260 persons aboard the airplane were fatally injured, as were 5 on the ground.

D. DETAILS OF THE EXAMINATION

This report documents the nondestructive inspection (NDI) of the vertical stabilizer and rudder. The vertical stabilizer was examined using ultrasonic inspection and Lamb wave imaging. Portions of the rudder were examined using x-ray radiography, Lamb wave imaging, thermography, ultrasonic inspection, and tap testing. The above inspections took place at NASA Langley, except for a portion of the tap testing and thermography of the rudder and ultrasonic inspection of the vertical stabilizer that were completed at Floyd Bennett Field in Brooklyn, New York. Pieces of the vertical stabilizer were inspected using x-ray computed tomography (CT scanning), and results from the CT scans will be presented in a separate report.

Several groups inspected the components using the above techniques. Representatives from the National Aeronautics and Space Administration's Langley Research Center (NASA Langley) completed the ultrasonic and Lamb wave imaging of the vertical stabilizer right and left skin panels. The ultrasonic imaging covered nearly the entire surface of each skin panel. They also inspected portions of the rudder using x-ray

radiography, Lamb wave imaging, and thermography. Results from these inspections are documented in Appendix A.

Representatives from Airbus Industrie completed hand ultrasonic inspections of the vertical stabilizer at the longitudinal and transverse attach lug areas, the lower ends of the spars, rib 1, and the rudder hinge attach locations on the aft spar. They also completed hand ultrasonic inspections of the rudder hinge attach blocks embedded in the rudder skin panels. They also performed ultrasonic imaging of the vertical stabilizer skin panels at the stringer locations using an ultrasonic phased array. Results from these inspections are documented in Appendix B.

Representatives from Iowa State University assisted by personnel from Sandia National Laboratory completed computer aided tap test (CATT) inspections, ultrasonic mechanical impedance analysis (MIA), and tap testing (woodpecker with a digital output) of the rudder at Floyd Bennett Field followed by additional CATT inspections of the rudder at NASA Langley. The locations of relative stiffness change were drawn on the skin panels in blue for the CATT inspection techniques and in red for MIA and woodpecker inspection techniques. These locations of stiffness changes as detected by each technique corresponded well. The results of the CATT inspections were integrated into an image map and are presented in Appendix C.

Representatives from Sandia National Laboratory completed an inspection of the lower end of the vertical stabilizer skin panels and the attachment lugs at Floyd Bennett Field. The inspections were conducted by hand and were difficult to interpret due to the complex geometry of the structure in the area. Where interpretation of the results was possible, the results corresponded well with those reported by NASA Langley and Airbus Industrie in Appendices A and B.

Representatives from Wayne State University completed several thermographic images of the rudder at Floyd Bennett Field, and results were similar to those presented in Appendix A.

Matthew R. Fox
Materials Engineer

E. APPENDIX A

NASA Langley Inspection of Rudder and Composite Tail from AA587

William P. Winfree
NASA Langley Research Center,
Hampton, VA

October 2, 2002

1. Ultrasonic Measurements

Ultrasonic imaging is a contact technique, where a scanner is placed on the vertical stabilizer (tail) surface, and a transducer is translated over the surface, to enable measurement of the ultrasonic response of the structure within the area of the scanner. For this case, an ultrasonic transducer is coupled to the composite using a closed tapered latex tube, filled with water. The surface of the region of the composite being inspected is kept moist, to ensure the ultrasound is able to couple from the tip of the latex tube into the composite. The same transducer is used to both generate and receive the ultrasonic wave. The output of the transducer is digitized at 100 Mhz and stored to enable post processing of the responses. A typical ultrasonic response is shown in figure 1.01.

One of the primary data reductions performed on the responses is a determination of the time of flight in the composite layer. The time of flight is delay time between the echo of the front surface of the composite and the echo off the back surface of the composite. In a homogenous material, the time of flight is proportional to the thickness of the material. Therefore a significant reduction in the time of flight is an indication of a delamination in the composite. If the composite thicknesses and velocity are known, it is possible to compare the time of flight measurements to calculations of the time of flight and be confident of the existence of delaminations. For this case there are two issues that make this determination difficult. First the thicknesses shown in the schematic drawings are significantly less than the thicknesses in the actual part. Second the velocity is not a constant in the part, but rather varies between the regions with and without stiffeners. Delaminations therefore are called out only when there is a significant relative change in the time of flight relative to the surrounding region that is not consistent the qualitative information in the schematics.

Another of the primary data reductions performed on the responses is a determination of the relative amplitudes of the echoes from the front and back surfaces. Reduction in the relative amplitude can be a factor of many parameters such as porosity in the composites, variations in coupling between the transducer and front surface of the composite and material mounted on the back surface of the composite. Since every variation in amplitude does not reflect a flaw in the composite, not all reductions in relative amplitude are noted in this documentation. However, for all significant changes in amplitude, the ultrasonic responses at that point were examined. A typical response that indicates an anomaly in the composite is shown in figure 1.02. For this point, there is clearly an echo between the front and back surface as noted in the figure. Where such echoes are clearly visible, the relative amplitudes of the region of are shown in detail.

Figures 1.03-1.23 are the results obtained from measurements on the left side of the tail. Figure 1.03 is the compilation of all the time of flight measurements performed on the left side. Two notable delaminations were detected at the lower end near the forward and aft spars. Enlarged images of the data with a designation of the extents of these two delaminations are shown in figure 1.04. Figure 1.05 designates the regions shown in figures 1.06 to 1.23. These are the images of regions with anomalies in the relative attenuation, with responses typical of those found in figure 1.02.

Figures 1.24-1.38 are the results obtain from measurements on the right side of the tail. Figure 1.24 is the compilation of all the time of flight measurements performed on the left side. No notable delaminations were detected on the right side of the tail. Figure 1.25 designates the regions shown in figures 1.26 to 1.38. These are the images of regions with anomalies in the relative attenuation, with responses typical of those found in figure 1.02.

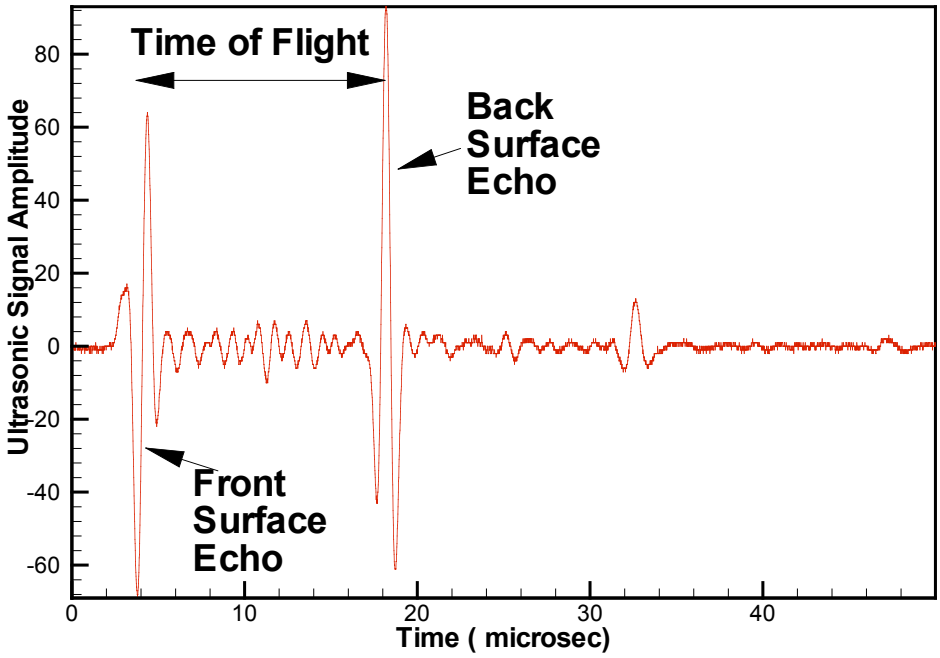

Figure 1.01 Typical time response of ultrasonic wave propagating in composite layer.

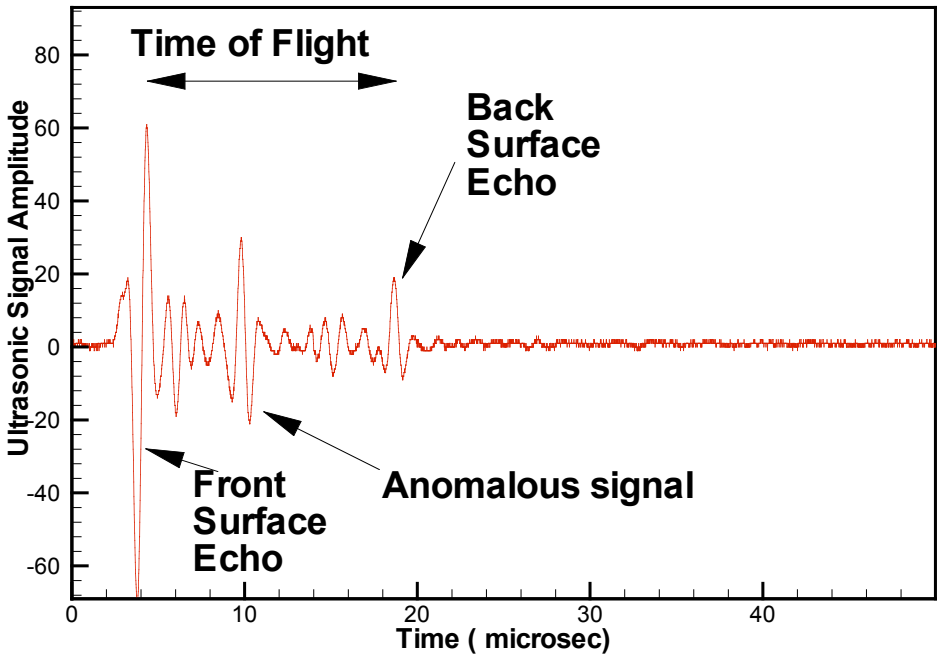

Figure 1.02 Typical ultrasonic signal from region of specimen with anomalous signal.

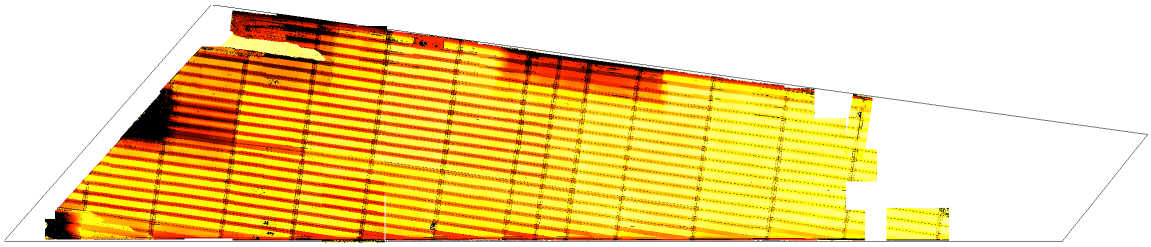

Figure 1.03 Ultrasonic time of flight measurements performed on the left side of the composite tail.

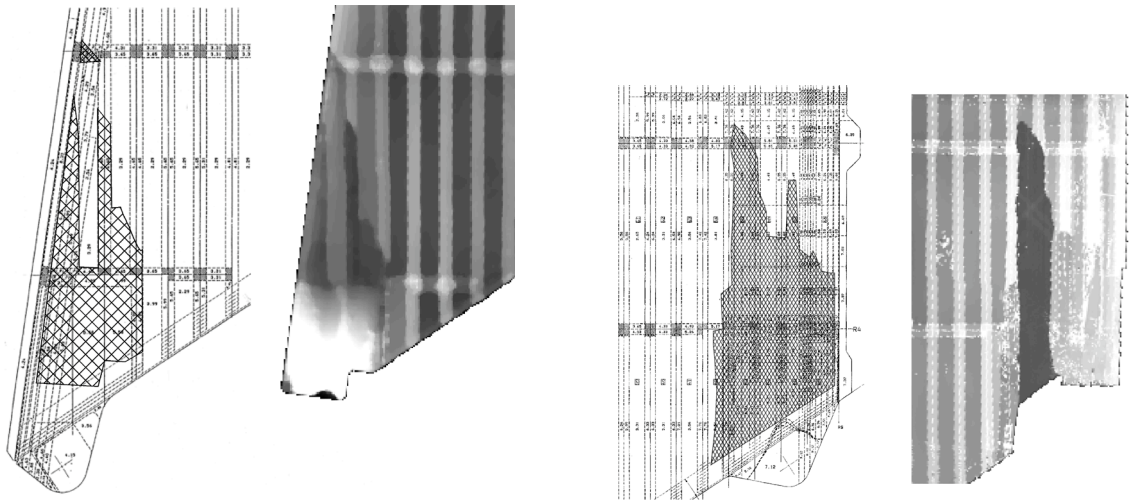

Figure 1.04 Expanded view showing delaminations at the lower end near the forward and aft spars.

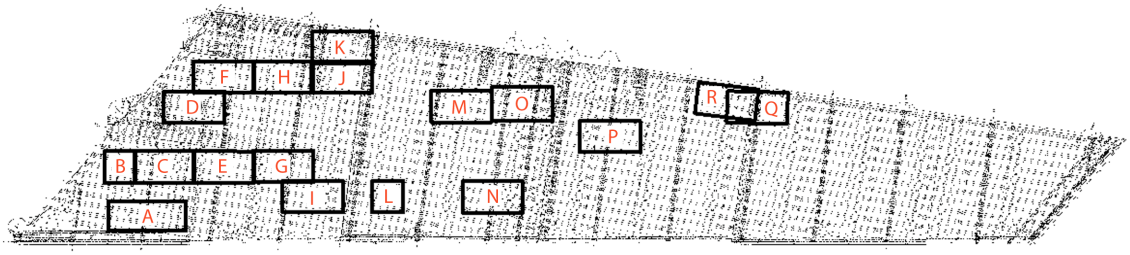

Figure 1.05 Region definitions used in subsequent images for the left side of tail. These are the regions with significant anomalies in ultrasonic attenuation responses.

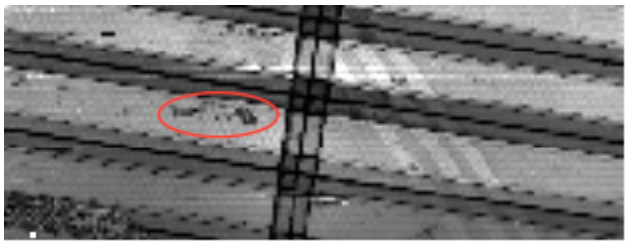

Figure 1.06 Ultrasonic attenuation image of left side tail region A.

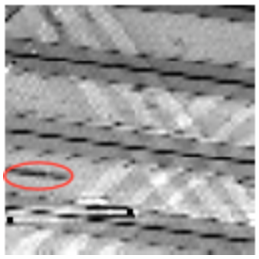

Figure 1.07 Ultrasonic attenuation image of left side tail region B.

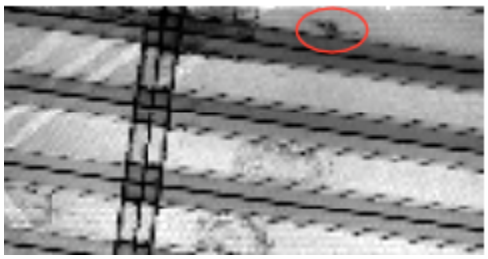

Figure 1.08 Ultrasonic attenuation image of left side tail region C.

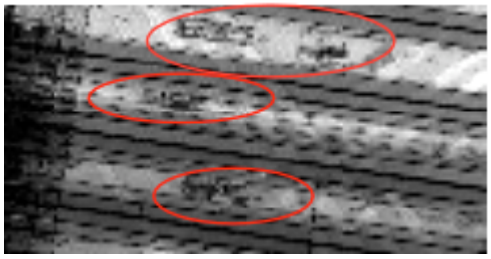

Figure 1.09 Ultrasonic attenuation image of left side tail region D.

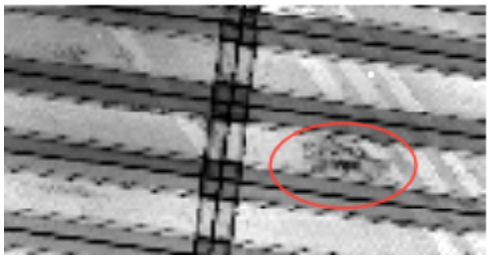

Figure 1.10 Ultrasonic attenuation image of left side tail region E.

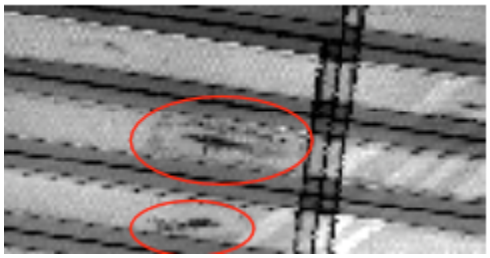

Figure 1.11 Ultrasonic attenuation image of left side tail region F.

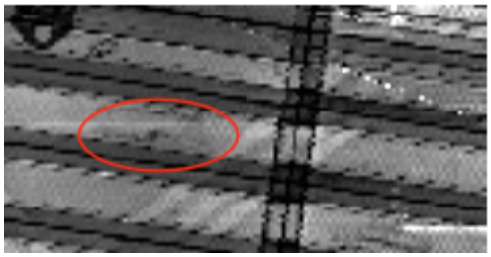

Figure 1.12 Ultrasonic attenuation image of left side tail region G.

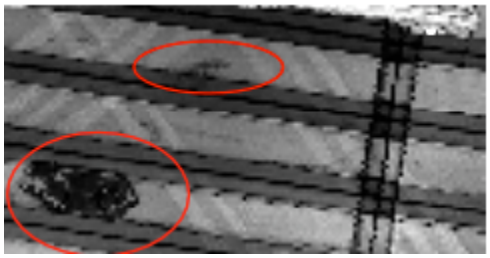

Figure 1.13 Ultrasonic attenuation image of left side tail region H.

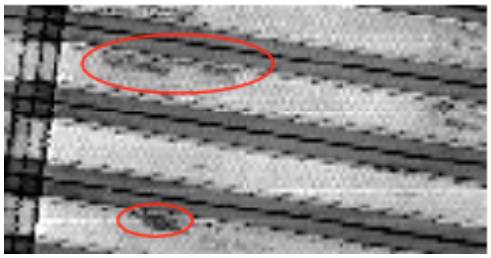

Figure 1.14 Ultrasonic attenuation image of left side tail region I.

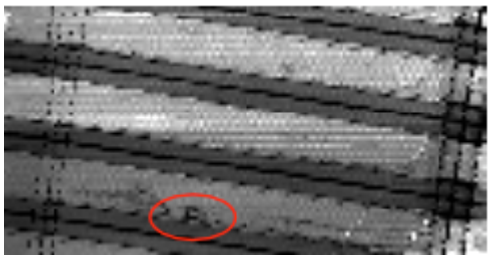

Figure 1.15 Ultrasonic attenuation image of left side tail region J.

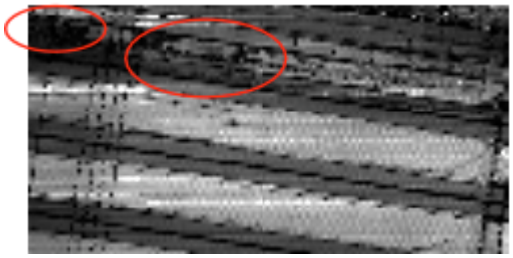

Figure 1.16 Ultrasonic attenuation image of left side tail region K.

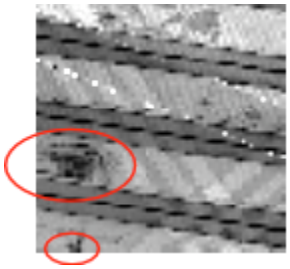

Figure 1.17 Ultrasonic attenuation image of left side tail region L.

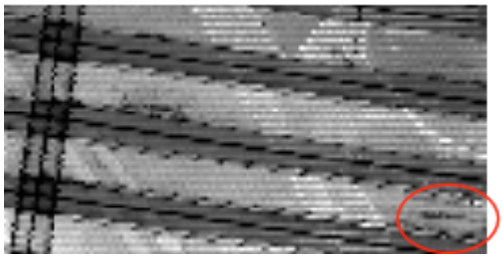

Figure 1.18 Ultrasonic attenuation image of left side tail region M.

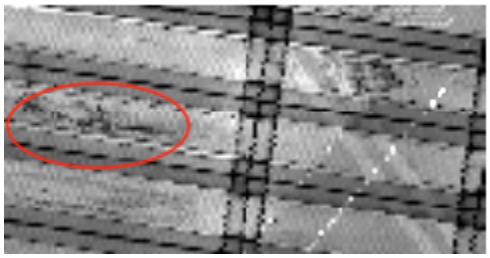

Figure 1.19 Ultrasonic attenuation image of left side tail region N.

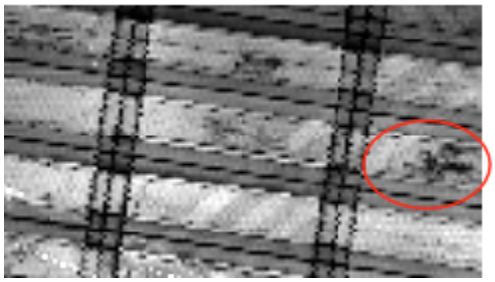

Figure 1.20 Ultrasonic attenuation image of left side tail region O.

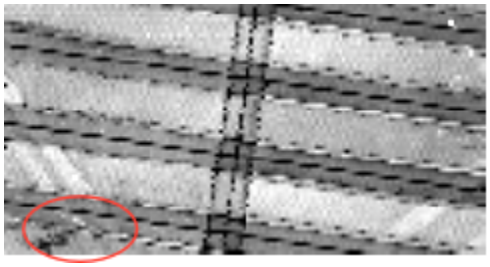

Figure 1.21 Ultrasonic attenuation image of left side tail region P.

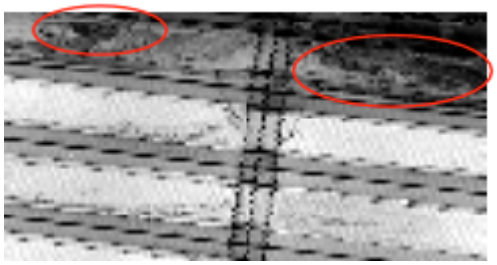

Figure 1.22 Ultrasonic attenuation image of left side tail region Q.

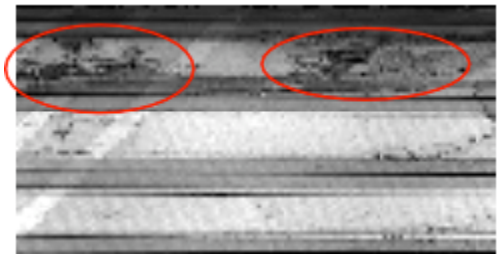

Figure 1.23 Ultrasonic attenuation image of left side tail region R.

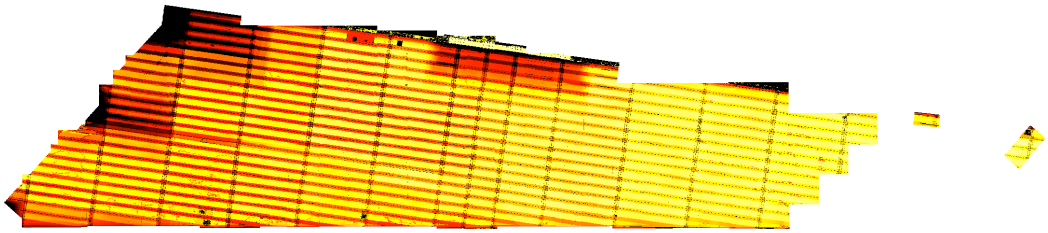

Figure 1.24 Ultrasonic time of flight measurements performed on the right side of the composite tail.

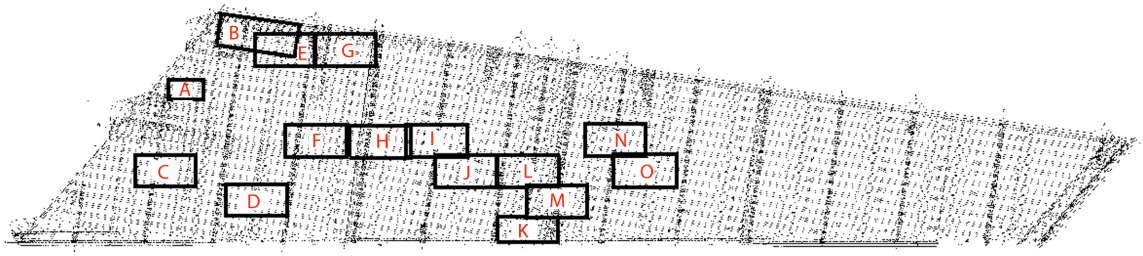

Figure 1.25 Region definitions used in subsequent images for the right side of tail. These are the regions with significant anomalies in ultrasonic attenuation responses.

Figure 1.26 Ultrasonic attenuation image of right side tail region A.

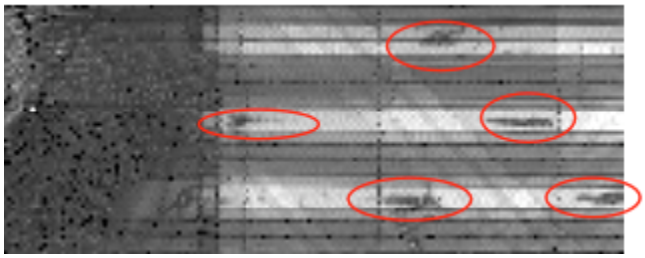

Figure 1.25 Ultrasonic attenuation image of right side tail region B.

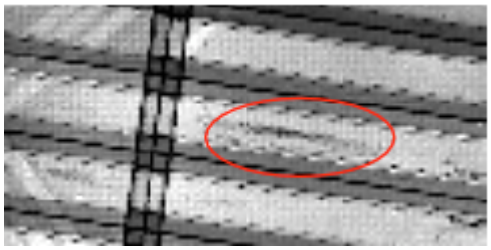

Figure 1.26 Ultrasonic attenuation image of right side tail region C.

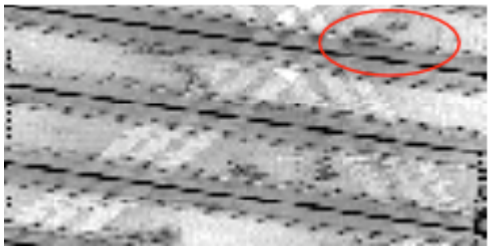

Figure 1.27 Ultrasonic attenuation image of right side tail region D.

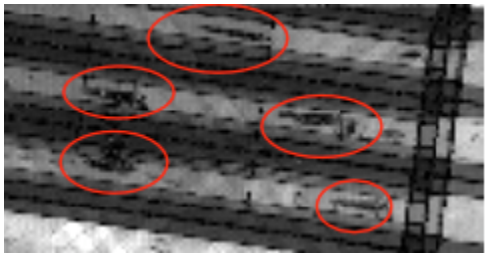

Figure 1.28 Ultrasonic attenuation image of right side tail region E.

Figure 1.29 Ultrasonic attenuation image of right side tail region F.

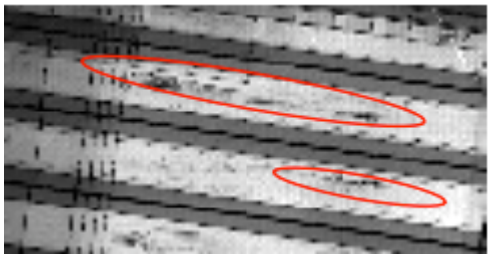

Figure 1.30 Ultrasonic attenuation image of right side tail region G.

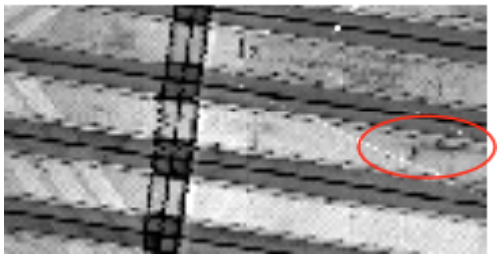

Figure 1.31 Ultrasonic attenuation image of right side tail region H.

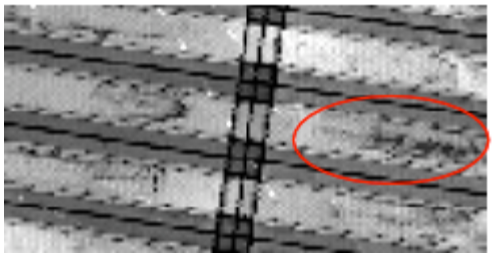

Figure 1.32 Ultrasonic attenuation image of right side tail region I.

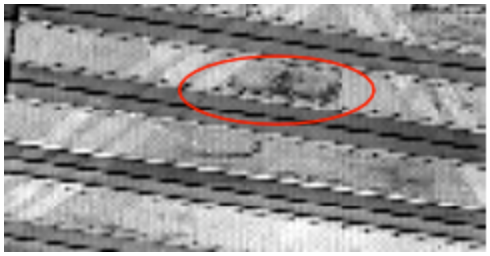

Figure 1.33 Ultrasonic attenuation image of right side tail region J.

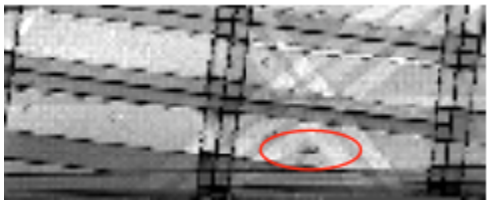

Figure 1.34 Ultrasonic attenuation image of right side tail region K.

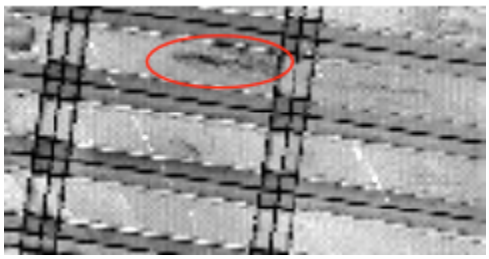

Figure 1.35 Ultrasonic attenuation image of right side tail region L.

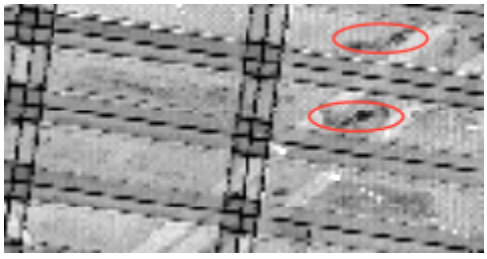

Figure 1.36 Ultrasonic attenuation image of right side tail region M.

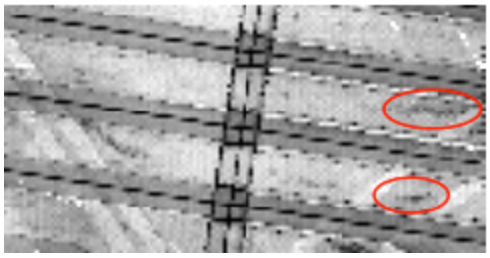

Figure 1.37 Ultrasonic attenuation image of right side tail region N.

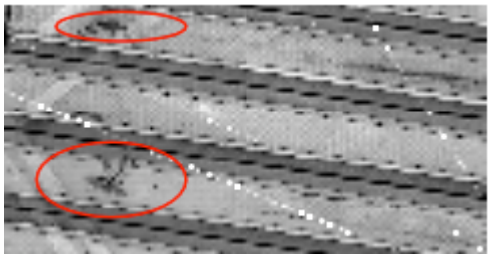

Figure 1.38 Ultrasonic attenuation image of right side tail region O.

2. Lamb wave inspection of composite tail

Among the emerging new technologies being developed for the inspection of composites is guided acoustic waves (Lamb waves). Studies have been conducted which show a reduction in Lamb wave velocity due to a loss of stiffness caused by matrix cracking. The system used for this test was the Lamb Wave ImagerTM (LWI); a commercial ultrasonic scanner developed by Digital Wave Corporation (DWC) in Englewood, Colorado. It is capable of measuring the elastic properties for isotropic as well as anisotropic materials. The system consists of a scanner, scanner control unit, a pair of transducers, and a computer. The scanning control and data analysis is performed by a commercial software package developed by DWC.

The scanner consists of a scan frame, a scan bridge, and a scan head. The scan frame dimensions are 20 inches wide by 24 inches long. The scan frame incorporates guide rods, a motor, and drive screw to control the motion along the y-axis. The scan bridge uses guides, a motor, and drive screw to govern the motion along the x-axis. The scan head is comprised of the ultrasonic transducers as well as a z-axis motor and a delta-x motor. The z-axis motor is used to raise and lower the transducers. Coupling between the article under test and the transducers is achieved through a thin rubber faceplate, which is attached to the bottom of the transducers. Bicycle tire patch material proved to be a convenient source for the rubber face plate and provided a good coupling between the test specimen and the transducers. A delta-x motor regulates the spacing between the stationary sending transducer and the movable receiving transducer.

The scanner control unit incorporates a receiver, a high-voltage amplifier, and a motor controller. The receiver has an amplification range from 0 to 66 dB. The high-voltage amplifier is used to amplify the pulse used to drive the sending transducer. It has a bandwidth of 12 kHz to 1 MHz and a maximum output of 350 volts peak-to-peak. The motor controller is capable of independently controlling the motion of each of the scanner motors. The computer contains a function generator card that produces a sinusoidal pulse and an 8-bit A/D board that digitizes the received signals.

Strips of data were acquired along the leading edges, trailing edges and along the center line of both the left and right side of the tail. Measurements were performed with a transducer separation of approximately 1 inch. The scan area for each scan was approximately 12 by 12 inches, and acquiring the data for each scan area required about 30 minutes.

A compilation of all the data from the right side superimposed on a schematic of the tail is shown in figure 2.01. The data from the left side is shown in figure 2.02. Regions of higher stiffness appear red, and lower stiffness regions appear orange in the figures. The most significant characteristics in the images are the variations in thickness of the composites tail. Aside from stiffness changes associated with thickness variations, there is no apparent evidence of any change in stiffness in the data.

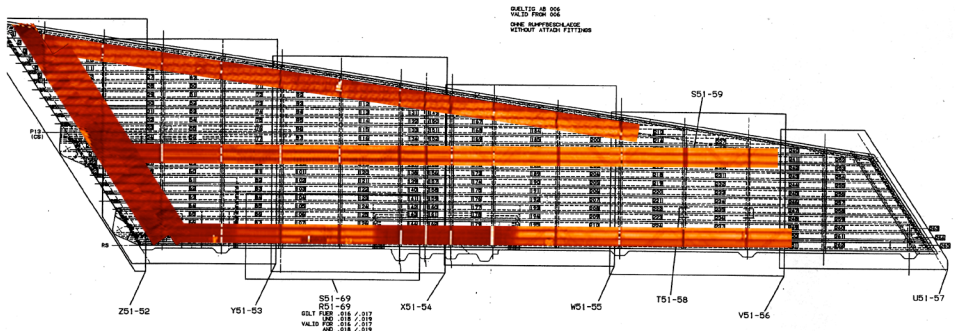

Figure 2.01 Lamb wave results for the right side of the composite tail.

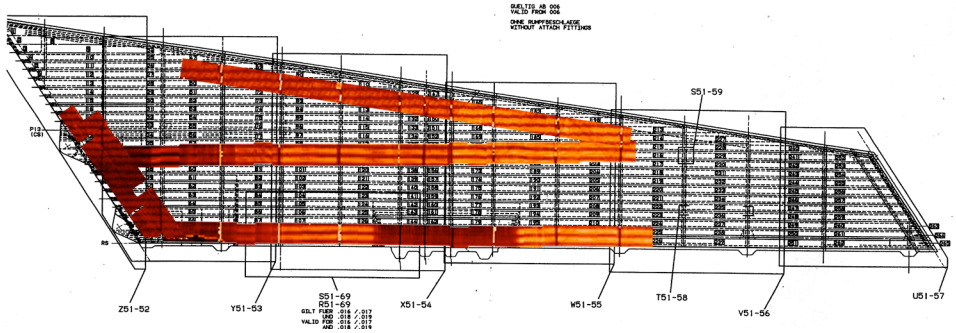

Figure 2.02 Lamb wave results for the left side of the composite tail.

3. X-ray radiography

X-ray radiography is a common technique for the detection of entrapped water in honeycomb structures. The water absorbs the x-rays reducing the intensity of the x-rays that expose the film. The reduction in the number of x-rays exposing the film results in a light spot on the film behind the water locations.

To perform the inspection, the rudder section was mounted vertically in two padded wooden yokes. Before the inspection, lead markers were taped to back side of the rudder. The lead markers are highly attenuative to x-rays and are clearly visible on the exposed film. By taking a picture of the position of the markers on the rudder, it is possible to determine the relative position of each piece of film with respect to the rudder.

An x-ray source was placed 8 feet from one side of the specimen, and four pieces of x-ray film are taped to the other side of the specimen. The x-ray source was turned on with a 30-kV acceleration voltage and a 2-minute exposure time. Following the exposure, the film was developed and examined to determine the location of water in the rudder.

A typical image is shown in figure 3.01. In the image, the entrapped water is clearly visible. Also visible in the image are the lead markers and the walls of the honeycomb. A compilation of all the photos is shown in figure 3.02. In the figure it is clear that the entrapped water is at the lower half of the rudder section.

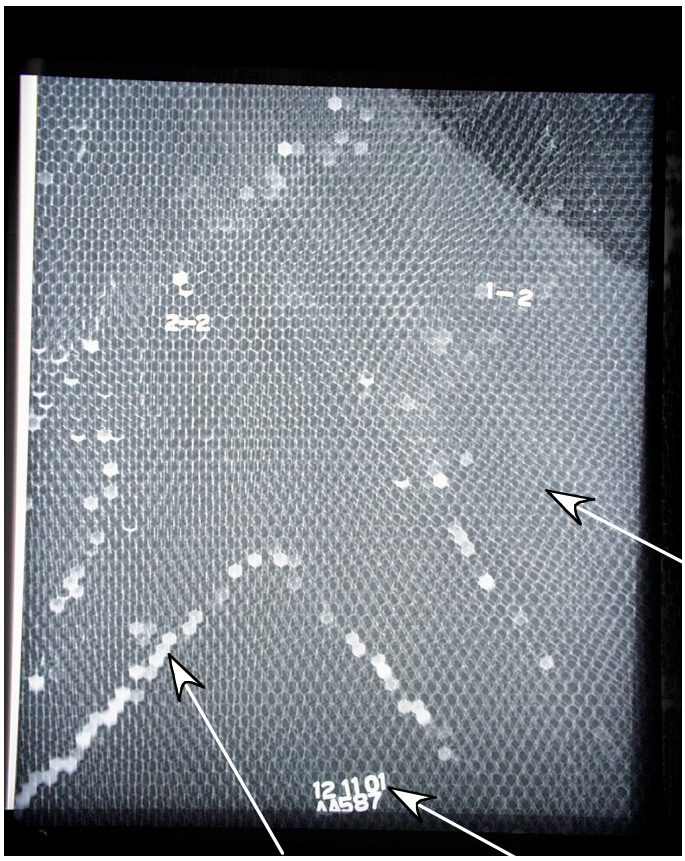

Figure 3.01 Radiographic image of water in honeycomb of rudder.

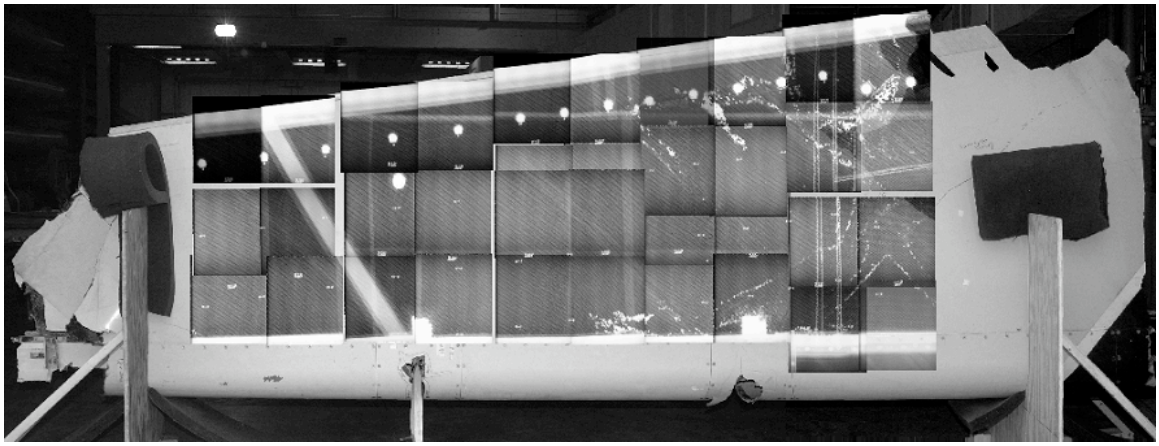

Figure 3.02 Compilation of radiography results superimposed on picture of the section of rudder examined.

4. Lamb wave imaging of rudder

Among the emerging new technologies being developed for the inspection of sandwich structure is guided acoustic waves (Lamb waves). Studies have been conducted which show a reduction in Lamb wave velocity due to a loss of bonding between the face sheet and subsurface honeycomb. The system used for this test was the Lamb Wave ImagerTM (LWI); a commercial ultrasonic scanner developed by Digital Wave Corporation (DWC) in Englewood, Colorado. It is capable of measuring the elastic properties for isotropic as well as anisotropic materials. The system consists of a scanner, scanner control unit, a pair of transducers, and a computer. The scanning control and data analysis is performed by a commercial software package developed by DWC.

The scanner consists of a scan frame, a scan bridge, and a scan head. The scan frame dimensions are 20 inches wide by 24 inches long. The scan frame incorporates guide rods, a motor, and drive screw to control the motion along the y-axis. The scan bridge uses guides, a motor, and drive screw to govern the motion along the x-axis. The scan head is comprised of the ultrasonic transducers as well as a z-axis motor and a delta-x motor. The z-axis motor is used to raise and lower the transducers. Coupling between the article under test and the transducers is achieved through a thin rubber faceplate, which is attached to the bottom of the transducers. Bicycle tire patch material proved to be a convenient source for the rubber face plate and provided a good coupling between the test specimen and the transducers. A delta-x motor regulates the spacing between the stationary sending transducer and the movable receiving transducer.

The scanner control unit incorporates a receiver, a high-voltage amplifier, and a motor controller. The receiver has an amplification range from 0 to 66 dB. The high-voltage amplifier is used to amplify the pulse used to drive the sending transducer. It has a bandwidth of 12 kHz to 1 MHz and a maximum output of 350 volts peak-to-peak. The motor controller is capable of independently controlling the motion of each of the scanner motors. The computer contains a function generator card that produces a sinusoidal pulse and an 8-bit A/D board that digitizes the received signals.

Measurements were performed with a transducer separation of approximately 2 inches. Measurements were only performed on portions of the rudder with enough residual strength to easily support the weight of the scan frame. A compilation of all the data from the right side of the rudder superimposed on a picture of the right side of the rudder is shown in figure 4.01. The data from the left side superimposed on the same picture is shown in figure 4.02. In regions with consist face sheet thickness, the areas with lower stiffness appear as lighter regions. Where there is an increase in ply thickness due to ply overlaps, these regions appear darker in the image. The system has difficulty tracking the delay time in the ultrasonic pulse in regions with significant addition subsurface support such as the lightning strip and rudder hinge attach blocks. For these regions, the stiffness maps are not meaningful. Figure 4.03 indicates typical responses in these regions.

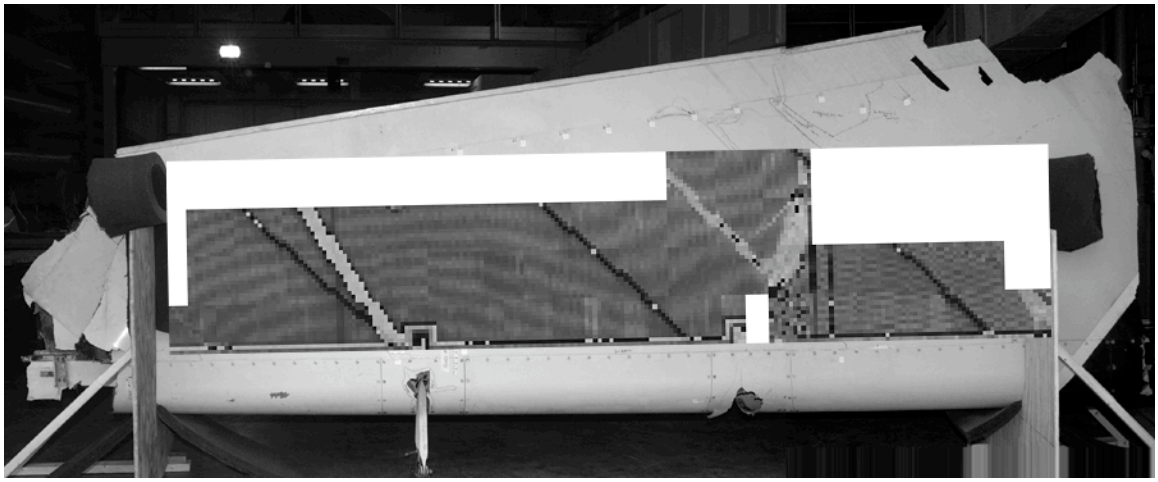

Figure 4.01 Lamb wave results on the right side of the rudder superimposed on a picture of the right side of the rudder.

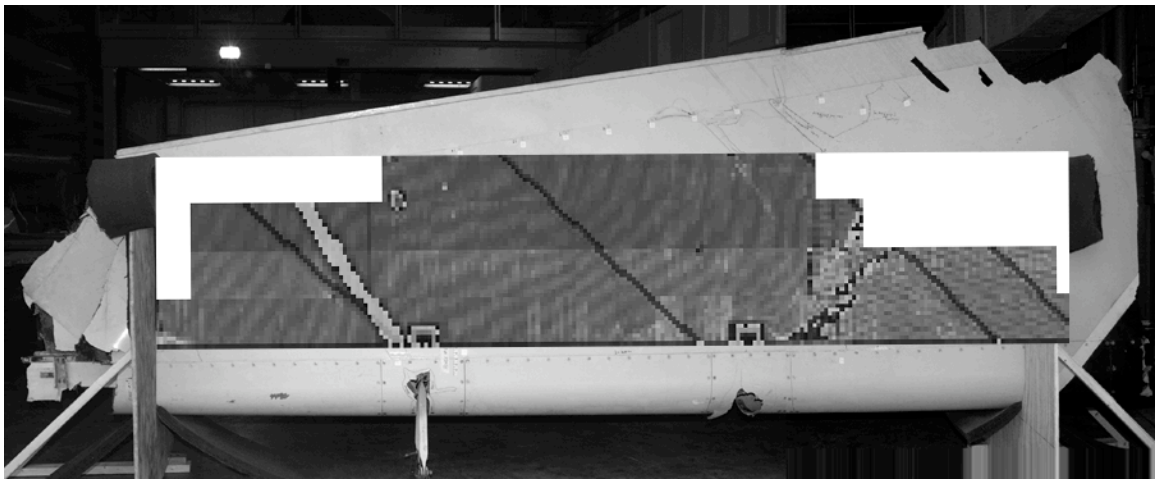

Figure 4.02 Lamb wave results on the left side of the rudder superimposed on a picture of the right side of the rudder.

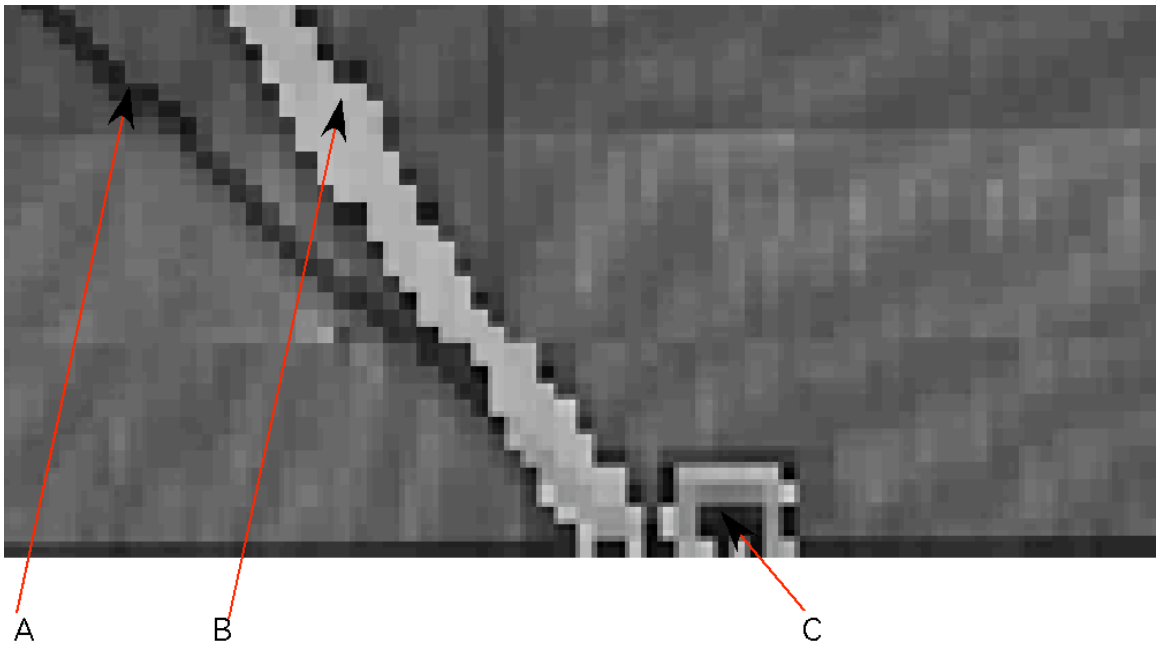

Figure 4.03 Identification of typical structural features in the Lamb wave image. A) Ply overlap, B) lightning strip and C) rudder hinge attach block.

5. Thermography of rudder

Thermography is a fast non-contacting inspection technique, particular useful for inspection of complex geometries. Subsurface variations in thermal properties change the pattern of the heat flow in the structure. These changes are detectable from the changes in temperature at the surface. By analyzing the pattern, it is possible to image subsurface features. This technique is particularly useful for imaging water in the rudder, where the thermal mass of the water acts as a thermal sink for the heat.

Measurement of the thermal response of the rudder was performed by impulse heating of one side of the specimen. The impulse heating was supplied by commercial photographic flash lamps. The duration of the flash was typically less than 3 msec. The time was much shorter than the data acquisition rate of the measurement system. The duration of the pulse is therefore inconsequential and can be considered as an impulse. A computer that controlled the measurement process triggered the application of the heat pulse.

Detection of the thermal response of the layer to impulse heating was performed with an infrared imager. The infrared imager used a detector array for the full field of view. The detector operated in the 3-5 μm range and is cooled to near liquid nitrogen temperatures with a closed cycle electric microcooler. The output of the imager was captured with a real time image processor. The sampling rate was variable down to 1/60 sec in steps of 1/30 sec. Variable length time records up to 300 time samples were obtainable with the system. User input into a computer, which controlled the measurement process, controlled the sampling time and the number of time samples. The computer typically recorded the infrared image of the specimen immediately prior to the firing of the flash lamps, then the thermal response of the specimen at a user-defined sampling rate and for a user-defined duration. Real time averaging of the thermal response also could be preformed to improve the signal-to-noise ratio. The thermal response was saved for post processing of the data to obtain a diffusivity map.

The thermal time response for a region of the rudder with and without entrapped water in the honeycomb is shown in figure 5.01. It is clear from the figure that there is significantly more cooling occurring in the region with entrapped water. The regions that appear darker in the data are indications of water. Other substructures, such as potting in the honeycomb also caused significant additional cooling relative to the unbacked face sheet. A compilation of all the data from the right side of the rudder superimposed on a picture of the right side of the rudder is shown in figure 5.02. The data from the left side superimposed on the same picture is shown in figure 5.03. Figures 5.04 and 5.05 show the same data with the locations of water highlighted in red.

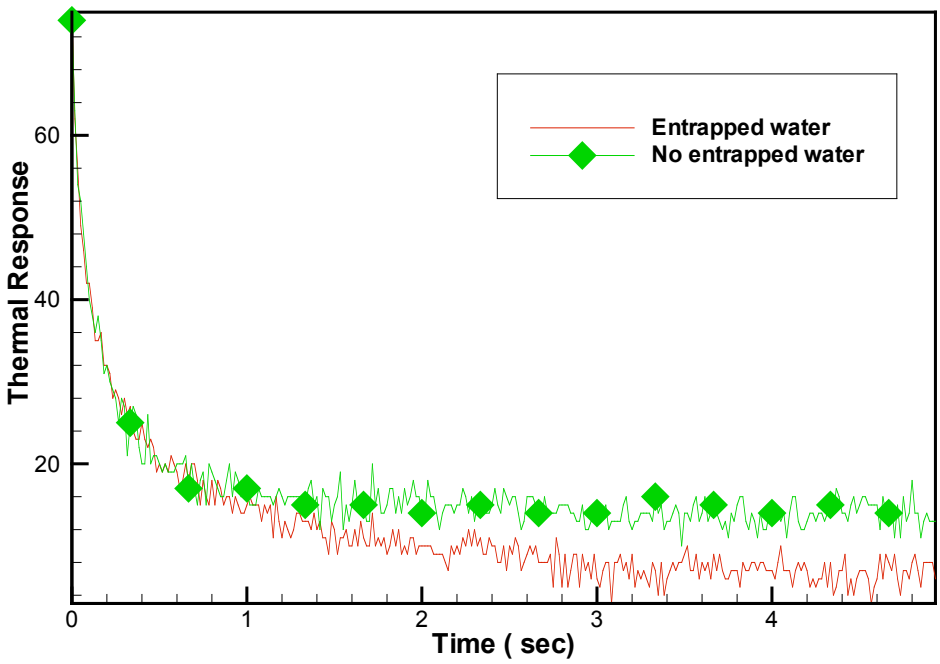

Figure 5.01 The thermal time response for a region of the rudder with and without entrapped water in the honeycomb

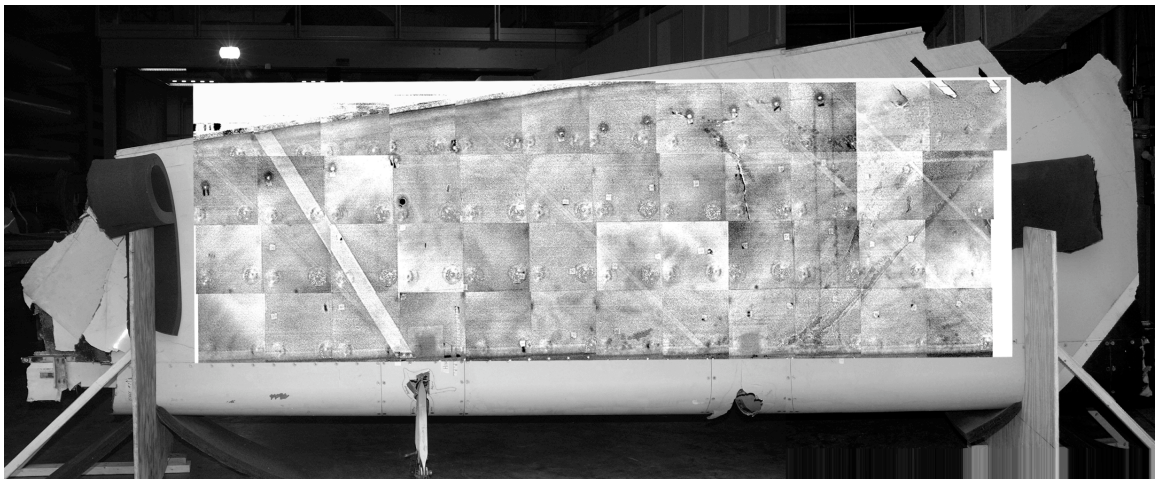

Figure 5.02 A compilation of all the data from the right side of the rudder superimposed on a picture of the right side of the rudder

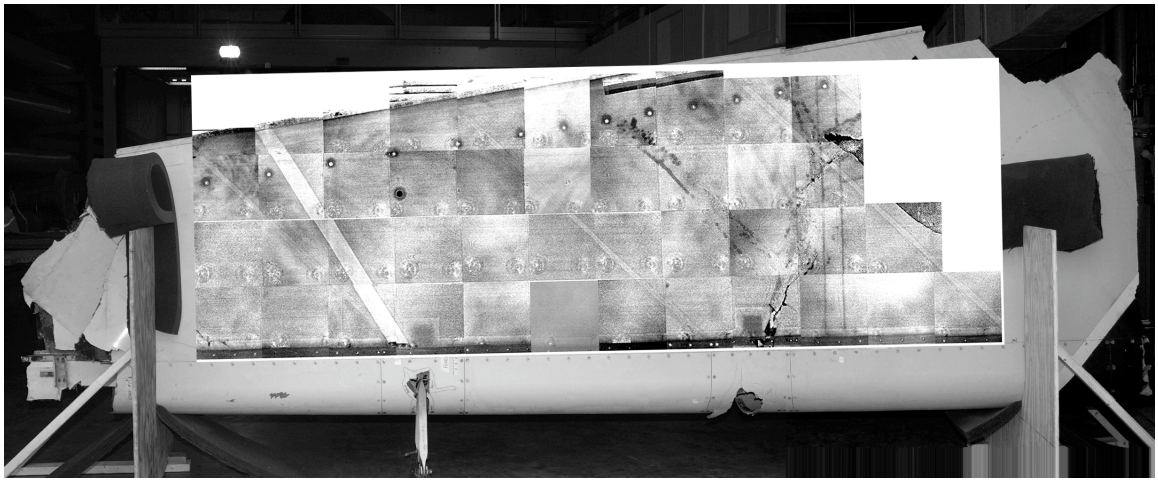

Figure 5.03 A compilation of all the data from the left side of the rudder superimposed on a picture of the right side of the rudder

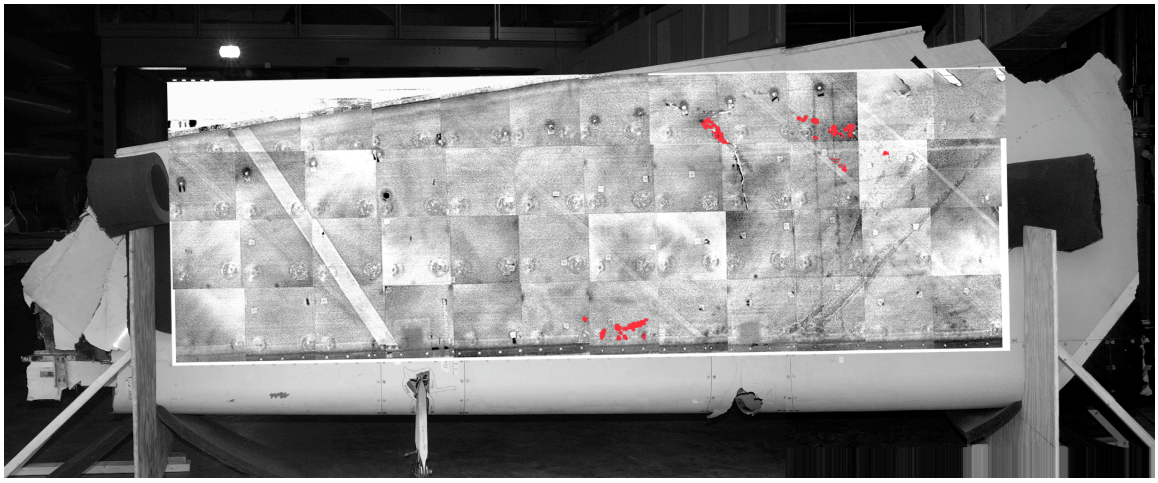

Figure 5.04 A compilation of all the data from the right side of the rudder superimposed on a picture of the right side of the rudder with water highlighted in red

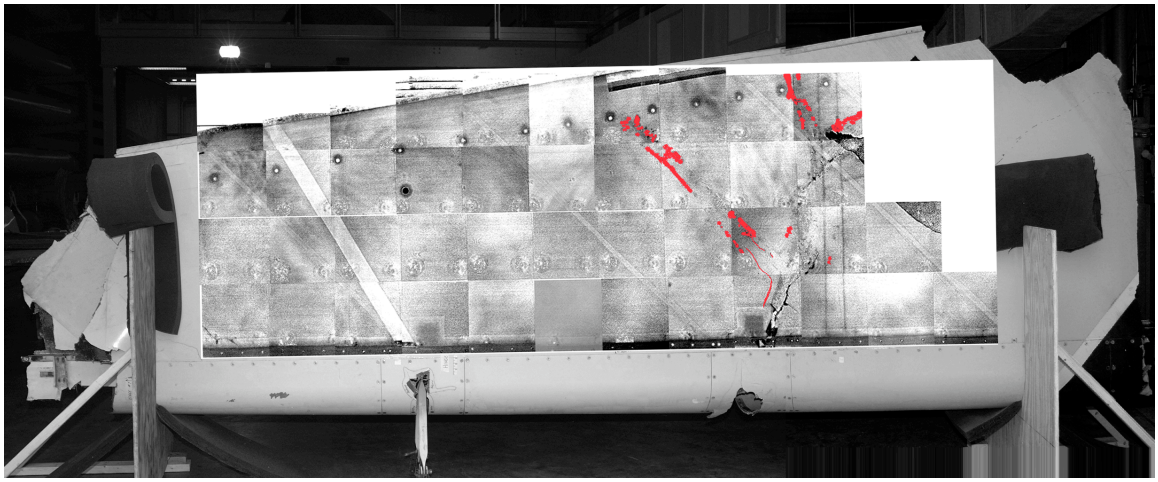

Figure 5.05 a compilation of all the data from the left side of the rudder superimposed on a picture of the right side of the rudder with water highlighted in red